

Magnetic properties of $\{M_4\}$ coordination clusters with different magnetic cores (M=Co, Mn).

Simona Achilli,^{*ab} Claire Besson,^c Xu He,^d Pablo Ordejón,^d Carola Meyer^e, Zeila Zanolli^{f,b,d}

We present a joint experimental and theoretical characterization of the magnetic properties of coordination clusters with an antiferromagnetic core of four magnetic ions. Two different compounds are analyzed, with Co and Mn ions in the core. While both molecules are antiferromagnetic, they display different sensitivities to external magnetic field, according to the different strength of the intra-molecular magnetic coupling. In particular, the dependence of the magnetization versus field of the two molecules switches with temperatures: at low temperature the magnetization is smaller in $\{Mn_4\}$, while the opposite happens at high temperature. Through a detailed analysis of the electronic and magnetic properties of the two compounds we identify a stronger magnetic interaction between the magnetic ions in $\{Mn_4\}$ with respect to $\{Co_4\}$. Moreover $\{Co_4\}$ displays not negligible spin-orbit related effects that could affect the spin lifetime in future antiferromagnetic spintronic applications. We highlight the necessity to account for these spin-orbit effects for a reliable description of these compounds.

1 Introduction

Molecular magnets constitute an excellent platform for molecular spintronics and quantum information storage and processing as their properties can be controlled at the nano/micro-scale during fabrication.¹⁻³ Coordination clusters formed by an inner magnetic core and a surrounding shell of organic ligands can be synthesized to control both the magnetic interactions between the ions within the molecule and the coupling between magnetic core and environment.⁴ Single-molecule magnets are particularly attractive for spin-dependent quantum transport applications⁵ as the spin retains its orientation in the absence of an external magnetic field and applications can leverage on the technology developed for functionalization with nanoparticles.^{6,7}

In recent years, research has concentrated on molecular magnets with large overall spin generated by ferromagnetic coupling between magnetic centers.⁸⁻¹⁰ On the other hand, the incorporation of molecular antiferromagnets in spintronic devices^{11,12} is still a new area of research. Recent proposals are only theoretical, and concern molecular AFM crystals¹³ or systems that can hardly be realized experimentally¹⁴. The expected advantages of antiferromagnetic coordination clusters are the same as for antiferromagnetic spintronic devices, i.e. robustness against perturbation due to magnetic fields, absence of stray fields, and capability to generate ultrafast dynamics and large magnetotransport effects.¹⁵ Antiferromagnetic molecules can be used to functional-

ize other organic systems, as carbon nanotubes, with the advantage that the current flowing through the tube does not alter the magnetic properties of the molecules^{16,17} and the low spin-orbit coupling allows long spin-flip lengths and spin lifetimes.

The application of molecular magnets in spintronics and quantum technologies would benefit from molecular design aimed at identifying the most suitable combinations of magnetic ions and organic ligands to ensure long spin coherence times, efficient spin injections and tunable transitions between spin states.¹⁸ In order to master this kind of applications, it is essential to understand the details of the magnetic interaction between the transition metal core ions and the subtle dependence of the magnetic properties of the molecule on the molecular structure.¹⁹ For example, Kampert et. al²⁰ showed that the magnetic properties of a family of $\{Mn_4\}$ antiferromagnets with the general formula $[(RCO_2)_4Mn_4L_2]$ (R=CF₃, CH₃, Ph, H₂L = 2,6-bis(1-(2-hydroxyphenyl)iminoethyl)pyridine) can be tailored by modifying the bridging carboxylate ligands, leading to a tunable exchange interaction between the magnetic ions. In this work we analyze the same molecular cluster with a different perspective by varying the chemical nature of the inner magnetic core. Through a joint experimental and theoretical characterization we compare the $\{Mn_4\}$ acetate complex with its cobalt analogue. While Mn^{II} centers are adequately described by the spin magnetic moment (spin-only model), Co^{II} centers in octahedral or pseudo-octahedral environments are characterized by significant orbital moments, leading to spin-orbit coupling (SOC) effects that could reasonably influence applications in more complex devices. Given the importance of magnetic fields in the study of spintronic devices, our experimental investigation mainly focuses on the changes in the magnetic properties of the complexes in an external magnetic field. The theoretical analysis, performed through a first-principles approach and a Heisenberg model Hamiltonian, is necessary to interpret the experiments and explain the differences between the two compounds, mostly due to the magnetic features of the magnetic core ions. Our computed spin dynamics highlights the key role played by electron correlation in the magnetic

^a Dipartimento di Fisica "Aldo Pontremoli", Università degli Studi di Milano, Via Celoria 16, Milan, Italy, simona.achilli@unimi.it

^b European Theoretical Spectroscopy Facilities.

^c Department of Chemistry, The George Washington University, Washington DC 20052, USA.

^d Catalan Institute of Nanoscience and Nanotechnology (ICN2), CSIC and BIST, Campus UAB, Bellaterra, 08193 Barcelona, Spain.

^e Department of Physics, Universität Osnabrück, 49076 Osnabrück, Germany.

^f Chemistry Department, Debye Institute for Nanomaterials Science, Condensed Matter and Interfaces, Utrecht University, PO Box 80 000, 3508 TA Utrecht, The Netherlands.

† Supplementary Information (SI) available: Full experimental details, Heisenberg fit of the SQUID data. Spin dynamics calculation. Relaxed structures

behavior of the complexes.

2 Methods

2.1 Theory

Theoretical calculations were performed in the Density Functional Theory (DFT) framework, using a pseudopotential description of the core electrons and atomic orbital basis set, as implemented in the SIESTA code.^{21,22} We adopted the local density approximation (LDA)^{23,24} for the exchange-correlation energy functional. A Hubbard correction for Mn and Co was included to account for the strong Coulomb interaction of localized *d* electrons. We use $U = 6$ eV for Mn and $U = 4$ eV for Co, according to the literature.^{20,25} To evaluate the role of spin-orbit coupling, which is relevant in Co, we also performed calculations including spin-orbit correction using the formalism of Ref.²⁶. The current version of the SIESTA code does not allow to simultaneously include Hubbard and spin-orbit corrections, thus the two effects are treated separately. The structure was relaxed with a tolerance on the forces on the atoms equal to 0.03 eV/Å. In the LDA+U calculations the fineness of the real-space grid (mesh-cutoff) was set to 400 Ry and the smearing of the electronic occupation (electronic temperature) to 100 K. In order to increase the accuracy in the convergence, SOC calculations were performed with 600 Ry mesh cutoff and 1K electronic temperature. The structural relaxation has been refined with SOC, starting from the LDA+U equilibrium geometry. The exchange coupling parameters $J_{i,j}$ were obtained by considering the lowest energy spin configurations of the Mn and Co centers and solving a system of equations (Heisenberg model) in the DFT energies with four $J_{i,j}$ parameters.

The geometry of the various spin configurations was kept fixed to the ground state one in order to exclusively account for the effect of the spin-flip on the total energy of the molecules.²⁷ Further, we exploited the model Heisenberg Hamiltonian $H = \sum_{i,j} \hat{S}_i \cdot J_{i,j} \cdot \hat{S}_j + \mu_B g \vec{S} \cdot \vec{B}$, where \hat{S}_i is the spin vector of atom *i* and *J* is the matrix of the exchange parameters, to fit experimental temperature and field-dependent magnetization data, as allowed by the implementation in the PHI code²⁸. In the following we label $J_1 = J_{1,4} = J_{2,3}$, $J_2 = J_{1,3} = J_{2,4}$, $J_3 = J_{1,2}$, $J_4 = J_{3,4}$, with the atoms numbered as indicated on Figure 1.

2.2 Experiment

The complexes $[M_4L_2(OAc)_4]$ ($M = \text{Mn, Co, Zn, } \{M_4\}$ for short), where $H_2L = 2,6\text{-bis-(1-(2-hydroxyphenyl)iminoethyl)pyridine}$, $HOAc = \text{acetic acid}$, and $M = \text{Mn}^{II}, \text{Co}^{II}$ or Zn^{II}) were synthesized by one pot reaction of 2-aminophenol, diacetylpyridine and manganese, cobalt or zincacetate, as described by Kampert *et al.* for the manganese complex,²⁰ with some modifications for the cobalt and zinc analogues. Full details of the synthesis methods are given in the ESI.†

The two new molecular complexes were characterized via single crystal diffraction conducted on a SuperNova (Agilent Technologies) diffractometer using Mo K radiation at 120 K. The crystals were mounted on a Hampton cryoloop with Paratone-N oil to prevent solvent loss. Thermogravimetric analysis was performed using a Mettler-Toledo TGA/SDTA 851e instrument with a heat-

ing rate of 10 K/min. Cyclic voltammograms were recorded in dry and deaerated acetonitrile solutions containing tetrabutylammonium perchlorate (0.1 M) as electrolyte and 3 mM of the analyte, using a SP-150 potentiostat (BioLogic Science Instruments) controlled by the EC-Lab software and a standard three-electrodes setup including a glassy carbon working electrode (diameter 3 mm), a platinum wire counter electrode and an Ag/AgNO₃ (0.1 M) reference electrode. Ferrocene was used as an internal standard. Magnetometry was performed on a Quantum Design MPMS-5XL SQUID magnetometer. The crystalline samples were crushed and placed under vacuum for 16 h before the complete removal of solvate molecules was checked by TGA. The resulting powders were compacted and immobilised into PTFE capsules. All data were corrected for the contribution of the sample holder (PTFE capsule). Measurements on $\{Zn_4\}$ were used to determine the diamagnetic susceptibility of this complex $\chi_{dia}(Zn_4) = -5.3 \times 10^{-9}$ m³/mol. The diamagnetic contribution in $\{Co_4\}$ and Mn_4 was then calculated from this value and Pascal's constants²⁹ for the Zn^{2+} , Co^{2+} and Mn^{2+} ions, yielding $\chi_{dia}(Co_4) = -5.1 \times 10^{-9}$ m³/mol and $\chi_{dia}(Mn_4) = -5.2 \times 10^{-9}$ m³/mol, and subtracted from the experimental susceptibility data.

3 Theoretical and experimental analysis

3.1 Synthesis and redox properties

The $\{M_4\}$, synthesized by one pot reaction of 2-aminophenol, diacetylpyridine and manganese, cobalt or zinc acetate, are stable towards oxidation in the solid state as well as in solution, despite the sensitivity of the $\{Co_4\}$ precursors to oxidation by O₂ during synthesis. This observation is confirmed by the cyclic voltammetry of the complex (Fig. 2), which displays two quasi-reversible ($\Delta E = 120$ mV) one-electron oxidation waves at 0.30 and 0.80 V vs. Fc^+/Fc which can be assigned as $\{Co_4^{II}\} \rightarrow \{Co_3^{III}Co^{II}\} \rightarrow \{Co_2^{II}Co_2^{III}\}$. As expected, the redox couples in the manganese complexes are shifted to lower potentials and show the large peak-to-peak characteristic of $Mn^{II}(HS) \rightarrow Mn^{III}(LS)$ processes. Finally, the zinc derivative shows irreversible ligand-centered oxidation processes above 0.5 V vs. Fc^+/Fc .

3.2 Molecular structure

The structure of the cobalt and zinc complexes was determined by single crystal X-ray diffraction to be analogue to that of the previously published manganese complex²⁰: the complexes consist of a cubic M_4O_4 core with two sets of two different ligand groups, for a total of 118 atoms (Fig. 1). The metallic core is a quasi-tetrahedron composed of two 7-coordinated ions (M_1, M_2) with pentagonal bipyramidal coordination and two 6-coordinated ions (M_3, M_4) with pseudo-octahedral symmetry.

The metal ions with the same coordination number are almost equivalent, as they overall face a quasi-identical chemical environment. The molecular cluster has an approximately C_2 symmetry and can be described as two identical structures on different planes that are rotated of 90° one respect to the other (Fig. 1), taking the rotation axis along *z*. Seven-coordinated M_1 and M_2 lie on different planes, each being connected in-plane to a pentadentate pyridine-diimine-diphenoxide type ligand (L^{2-}), completed

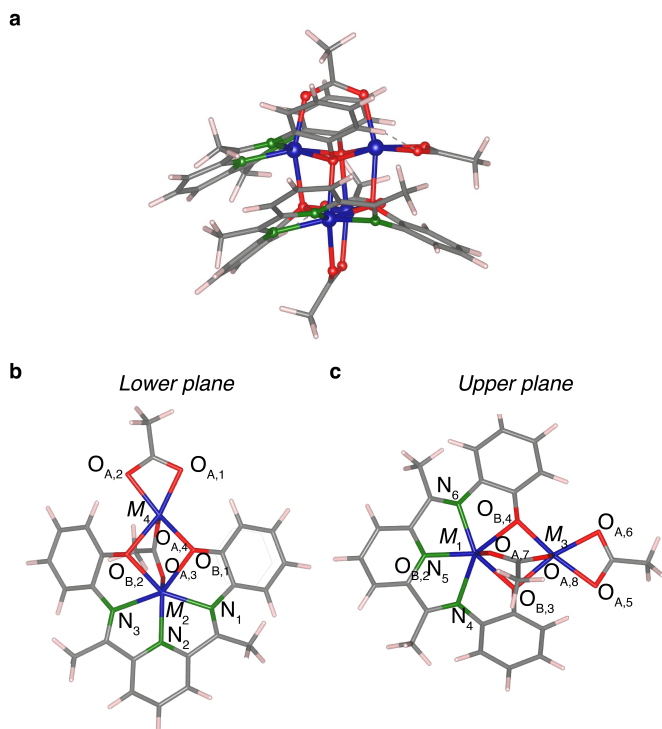


Fig. 1 Molecular structure of the M_4 complex. a) side view. Blue: Mn, Co or Zn atoms; red: O; green: N; gray: C, white: H. b) top view of the lower half of the molecule. c) top view of the upper half of the molecule. Relaxed coordinates are available in ESI.

by the oxygen of a bridging acetate and a κ^3 phenoxide oxygen from the other L^{2-} ligand. The coordination sphere of M_3 , M_4 is a pseudo octahedron of six oxygen atoms provided by a bidentate acetate ligand, the other oxygen of the two bridging acetate and two phenoxide oxygen from the L^{2-} ligand. (Relaxed coordinates available in ESI).

The inner cage of the three molecules is composed by four transition metal ions with different atomic valence configurations, $3d^5$ for Mn(II), $3d^7$ for Co(II) and $3d^{10}$ for Zinc(II). The latter complex is therefore diamagnetic; it was used experimentally to determine the diamagnetic contribution to the susceptibility of the complexes and will not be discussed further. Both Mn(II) and Co(II) ions display high spin configurations, i.e. $S=5/2$ for Mn and $S=3/2$ for Co.

Despite the similarity between the structures of the manganese and cobalt complexes, experimental evidence and DFT calculations show small differences in bond lengths in the inner core. In agreement with the larger atomic radius of Mn with respect to Co, the $\{Mn_4\}$ central cage is slightly larger than the $\{Co_4\}$ one, due to larger M-O and M-N bond-lengths. Details of the structure are reported in Table 1.

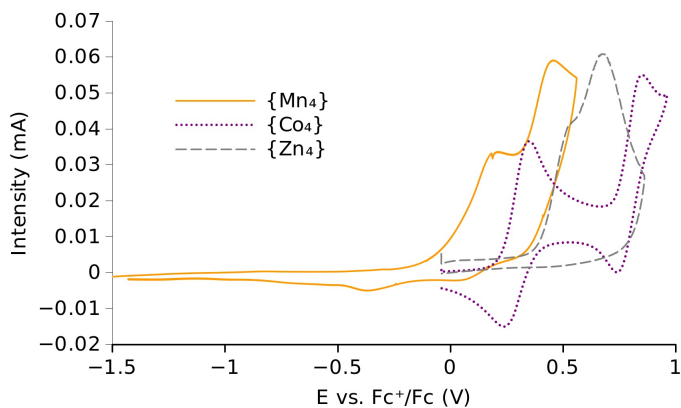


Fig. 2 Cyclic voltammograms of the $\{M_4\}$ complexes ($M = Mn, Co, Zn$, concentration ca. 3 mM) in acetonitrile. Tetrabutylammonium perchlorate (0.1 M) is used as electrolyte and the scan rate is 50 mV/s.

Table 1 Theoretical (DFT) and experimental (XRD) bond-lengths (\AA) of the $\{Mn_4\}$ and $\{Co_4\}$ molecular complexes. XRD data was obtained at 208 K for $\{Mn_4\}$ ²⁰ and at 100 K for $\{Co_4\}$.

$d(\text{\AA})$	M_1-M_2	M_3-M_4	$M_1-M_3^a$	$M_2-O_{B,1}^b$	$M_4-O_{A,2}^b$
$\{Mn_4\}$					
DFT	3.35	3.45	3.64/3.65	2.20-2.30	2.15-2.22
XRD	3.62	3.47	3.50/3.55	2.27-2.31	2.21-2.22
$\{Co_4\}$					
DFT	3.26	3.21	3.42/3.44	2.15-2.21	2.07-2.11
XRD	3.39	3.19	3.15/3.16	2.17-2.29	2.11-2.19

a: The two values correspond to the equivalent pairs of atoms.

b: Range given for all equivalent distances in the complex.

3.3 Behavior in magnetic field

In order to quantify the strength of the magnetic interaction within the molecule and the response to an external magnetic field we performed SQUID magnetometry experiments (Fig. 3). A singlet ground state is observed in both complexes, indicating the presence of antiferromagnetic coupling between the magnetic ions in the molecule. The molecular moment μ_{mol} as a function of magnetic field ($H = 0 - 5$ T) and temperature ($T = 20 - 300$ K) was fitted to a mean field model (Curie-Weiss law, equation 1), yielding Néel temperatures of $T_N = 23$ K for $\{Mn_4\}$ and $T_N = 12$ K for $\{Co_4\}$:

$$\mu_{mol} = \frac{C H}{T - T_N} \quad (1)$$

Those values, as well as the larger slope of the molecular moment at low field/low temperature observed for $\{Co_4\}$ in comparison to $\{Mn_4\}$, suggests that the antiferromagnetic coupling between the metal atoms in $\{Co_4\}$ is smaller than in $\{Mn_4\}$. Notably, the behavior is reversed at high temperature with a larger magnetic moment for $\{Mn_4\}$ than for $\{Co_4\}$, which is in agreement with the higher spin moment of the Mn centers.

The Curie constant C obtained for the $\{Mn_4\}$ complex ($3.0 \times 10^{-3} \mu_B \cdot K \cdot Oe^{-1}$) is in good agreement with a spin-only model ($3.1 \times 10^{-3} \mu_B \cdot K \cdot Oe^{-1}$ for $g = 2$ and $S = 5/2$). Such a model is not adequate for octahedral cobalt(II) complexes, with their $^4T_{1g}$

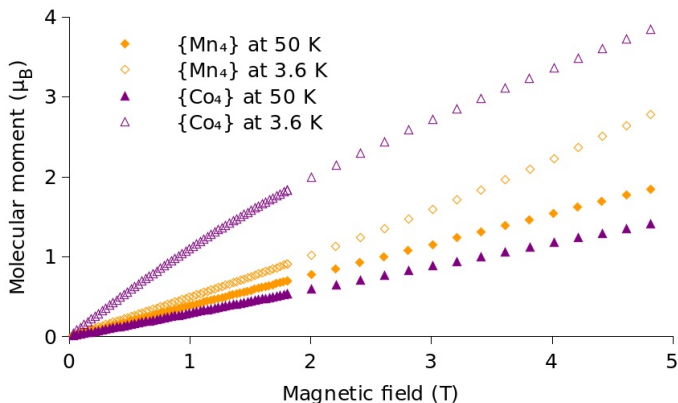


Fig. 3 SQUID magnetometry data of $\{\text{Mn}_4\}$ (orange) and $\{\text{Co}_4\}$ (purple) at $T=3.6$ K (open symbols) and $T=50$ K (filled symbols).

ground term, and effective orbital momentum $L = 1$.³⁰ Indeed, the Curie constant of $\{\text{Co}_4\}$ ($2.4 \times 10^{-3} \mu_B \cdot \text{K} \cdot \text{Oe}^{-1}$) obtained from the Curie-Weiss fit deviates significantly from the one calculated by the spin-only model ($1.3 \times 10^{-3} \mu_B \cdot \text{K} \cdot \text{Oe}^{-1}$).

The measured magnetic susceptibility is reported in ESI, together with the theoretical one obtained from spin dynamics calculations. The agreement between theory and experiment is fairly good in the LDA+U approximation (see the discussion in 3.6).

3.4 Magnetic and electronic properties

In order to characterize the magnetic configuration of the inner cage and to ascertain the role of spin-orbit coupling in $\{\text{Co}_4\}$ we performed ab initio calculations. DFT analysis shows that the ground state is characterized by an antiferromagnetic coupling between non-equivalent metal ions (M_1/M_3 and M_2/M_4), and a ferromagnetic one between the equivalent pairs (M_1/M_2 and M_3/M_4) giving rise to a up-up-down-down (*uudd*) configuration, referring to the relative alignment of the spins of the four metal ions. The magnetic moments of Co, Mn, N and O in the two molecular complexes, deduced from the Mulliken charge population, are reported in Table 2. Due to the chemical interaction with the ligands the magnetic moment of the metal atoms in the molecular complexes is reduced with respect to the isolated ions ($\sim 4\%$ in $\{\text{Mn}_4\}$, $\sim 10\%$ $\{\text{Co}_4\}$). Accordingly, the induced magnetization of the ligands is smaller for $\{\text{Mn}_4\}$ than for $\{\text{Co}_4\}$, as can be appreciated also through the small differences in the spatial distribution of the spin density ($\rho_{up} - \rho_{down}$ on the oxygen atoms, Fig. 4). In $\{\text{Mn}_4\}$ the magnetic moment of bridging oxygens (O_A and O_B) is negligible. In $\{\text{Co}_4\}$ the bridging phenoxy oxygens have opposite magnetization: O_{B2} and O_{B3} are magnetized up while O_{B2} and O_{B3} are magnetized down. Out of the eight acetate oxygens O_A , only two (O_{A+}) display a small positive magnetic moment while the other six (O_{A-}) have a larger (in modulus) negative magnetic moment (mean value reported in Table 2). The average magnetization of the N atoms is comparable to the average contribution of O_A but with opposite sign. As a consequence, despite the presence of local magnetic moments,

Table 2 Magnetic moment (μ_B) of the $\{\text{Mn}_4\}$ and $\{\text{Co}_4\}$ molecular complexes. Average values are reported for N (variance $0.004 \mu_B$), and O_A atoms with positive ($O_{A+} = O_{A_{3,7}}$) and negative ($O_{A-} = O_{A_{1,2,4,5,6,8}}$) magnetic moment (variances in $\{\text{Mn}_4\}/\{\text{Co}_4\}$ are $0.0/0.001 \mu_B$ and $0.001/0.002 \mu_B$, respectively). Note the (anti)ferromagnetic coupling between (non-)equivalent metal ions: $M_1 \sim -M_3$, $M_2 \sim -M_4$, $M_1 = M_2$, $M_3 = M_4$.

(μ_B)	$M_{1,2}$	$M_{3,4}$	N	O_{A+}	O_{A-}	$O_{B_{2,3}}$	$O_{B_{1,4}}$
$\{\text{Mn}_4\}$	4.82	-4.89	0.01	0.01	-0.01	0.00	0.00
$\{\text{Co}_4\}$	2.71	-2.73	0.05	0.03	-0.04	0.02	-0.02

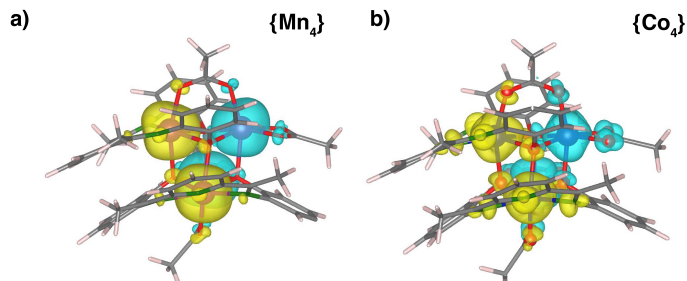


Fig. 4 Spin density on $\{\text{Mn}_4\}$ and $\{\text{Co}_4\}$. Yellow (blue) isosurfaces correspond to positive (negative) values with a fixed value of 0.025. Spin density on the ligands is more pronounced in the $\{\text{Co}_4\}$ case.

the total spin of both molecules is $S_{TOT} = 0$ confirming their antiferromagnetic character. Nevertheless, the major spread of the magnetic moment observed in $\{\text{Co}_4\}$ is an indication of a possible large magnetic interaction of this molecule with other systems when the complex is used for functionalization.

In Figure 5 the DOS of the two molecules projected on different atoms of the complex (PDOS), is reported. The PDOS of Mn ions is characterized by a single spin population, due to the almost complete filling of the spin-up $3d$ electrons. In Co, instead, majority and minority spins are present, according to the more-than-half filling of the $3d$ orbitals. The oxygen atoms display a different PDOS depending on the group they are attached to. In particular the states of the bridging oxygen atoms O_B partially overlap with the states of the magnetic ions, with larger extent for the seven-coordinated ones ($M_{1,2}$) in the majority-spin component and with the six-coordinated ones ($M_{3,4}$) in the minority spin component. This overlap, which appears to be slightly more intense in $\{\text{Mn}_4\}$, is responsible for the coupling between magnetic ions via superexchange interaction mechanism.³¹

For both complexes, the O_A atoms are characterized by majority spin states in the $[-3, -1]$ eV energy range and minority states centered around -2.5 eV, with a moderate overlap with the metal atoms in both cases.

We can therefore conclude that they contribute to the magnetic coupling between metal centers with a similar strength.

The hybridization with states of the ligands is also responsi-

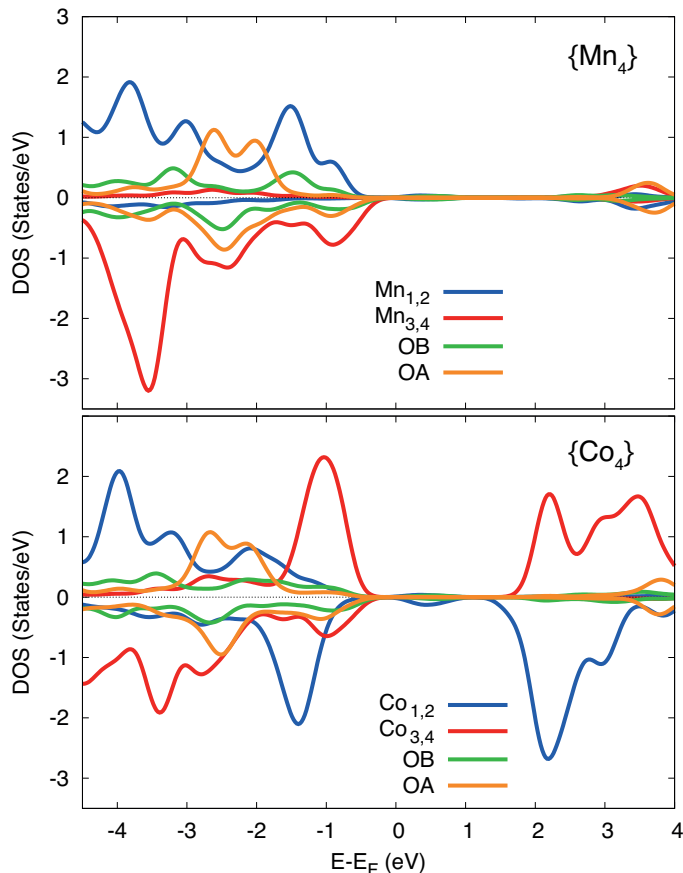


Fig. 5 Density of states projected on the magnetic ions and different oxygen atoms (O_A and O_B) in the two molecular complexes. The average PDOS per atom type is reported.

ble for the charge transfer from the magnetic ions to the nearby atoms. In the molecular complexes, Mn and Co atoms display a number of electrons smaller than the valence of the isolated atom, as reported in Table 3 in term of the net atomic charge, i.e. they donate electron charge. This reduction of charge is larger for the two metal ions bound to the pyridine-diimine group ($M_{1,2}$) with respect to the 6-coordinated magnetic atoms in the same molecule ($M_{3,4}$). Moreover, the percentage of lost charge is larger in $\{Mn_4\}$ ($\sim 25\%$) than in $\{Co_4\}$ ($\sim 22\%$), according to the larger hybridization with the surrounding coordination groups. The oxygen atoms act as electron acceptors in both molecules. The maximum charge transfer is toward the bridging oxygens that acquire 0.60 and 0.68 electrons (mean values) in $\{Mn_4\}$ and $\{Co_4\}$, respectively. For O_A atoms the absolute values of the acquired charge ($\sim 0.4e$) are similar in the two complexes. N atoms participate to charge transfer towards the ligands by donating electrons, with a slightly larger fraction in $\{Mn_4\}$ ($\sim 0.29e$) than in $\{Co_4\}$ ($\sim 0.21e$). On the basis of the results reported by Kampert et al.²⁰ the charge withdrawn from the $[M_4O_4]$ core (by the ligands) is inversely proportional to the strength of the magnetic interaction within the complex. For both complexes, the analysis of Mulliken charges predicts that the $[M_4O_4]$ core acts as a donor, with 2.45

Table 3 Net atomic charges of the atomic species in the $\{Mn_4\}$ and $\{Co_4\}$ molecular complexes (in units of electron charge e). Positive (negative) values indicate donor (acceptor) behavior. Average values are reported for the equivalent centers.

$\Delta q(e)$	$M_{1,2}$	$M_{3,4}$	N	O_A	O_B
$\{Mn_4\}$	+1.10	+1.32	+0.29	-0.39	-0.60
$\{Co_4\}$	+1.49	+1.63	+0.22	-0.44	-0.70

and 3.43 electrons donated in the Mn and Co case, respectively. Therefore, we expect that a stronger antiferromagnetic coupling in $\{Mn_4\}$ than in $\{Co_4\}$, supporting the experimental findings.

3.5 Role of Spin Orbit Coupling

In the previous paragraphs we have analyzed the results obtained with the LDA+U approximation, necessary to account for the electronic correlation of localized $3d$ orbitals, but limited in the SIESTA code to a collinear-spin description of magnetism. This approximation is valid for the Mn(II) ions, as the high-spin d^5 electronic configuration does not have a net orbital momentum. In Co(II) centers, instead, the d^7 configuration leads to an orbital momentum $L=3$ for an isolated ion. While the orbital momentum is quenched in low symmetry environments, including pentagonal bipyramidal, it is not in a perfect octahedron, where $L=1$. As two of the metal centers in $\{Co_4\}$ display a pseudo-octahedral geometry, SOC is expected to have a significant effect on the magnetic properties of this complex.

In order to investigate the role of SOC in the complexes, we have performed DFT calculations including SOC for both molecules at $U = 0$ using the fully relativistic pseudopotential formalism³² implemented in SIESTA²⁶. The magnetization direction has been set along the z axis for $\{Mn_4\}$. Indeed we verified that for this molecule the magnetic anisotropy related to spinflip along five independent directions is at most $\sim 100 \mu eV$ per molecule. For $\{Co_4\}$, which is expected to display strong spin-orbit effects, we have explored 30 different direction of the magnetization. The easy axis for $\{Co_4\}$ is rotated with respect to the z direction with a polar angle 150° and azimuthal angle 45° . The maximum magnetic anisotropy for spinflip amounts to 12 meV per molecule. The results reported below are relative to $\{Co_4\}$ with the spin along the easy axis.

In Table 5 and 4 the computed S, L, and their sum (J) are reported for both molecular complexes. In both cases, the atomic spin is slightly reduced with respect to the LDA+U calculation. The four metal ions in $\{Co_4\}$ display an orbital moment which is smaller than the value expected for the isolated ion, but significantly larger than the manganese analogue. The quenching is stronger for the two ions in the pentagonal bipyramidal coordination, for which $\sqrt{\langle L^2 \rangle} = 0.11$. For the 6-coordinated pseudo-octahedral Co ions L is not negligible (~ 0.4) and contributes to an overall value of $\sqrt{\langle J^2 \rangle} \sim 3$.

On the basis of these results we can infer that Spin-Orbit coupling plays a crucial role in determining the magnetic properties of $\{Co_4\}$ while it is less relevant in $\{Mn_4\}$ and in the latter case it can be disregarded.

Table 4 Spin (S), orbital moment (L) and their composition (J) for the four magnetic atoms of the $\{\text{Mn}_4\}$ core. The data are reported in units of μ_B .

	Mn ₁	Mn ₂	Mn ₃	Mn ₄
$\sqrt{\langle S^2 \rangle}$	4.33	4.37	4.34	4.34
S _x	1.43	-1.35	0.17	0.37
S _y	1.097	-0.59	-0.20	0.058
S _z	3.94	4.11	-4.33	-4.32
$\sqrt{\langle L^2 \rangle}$	0.052	0.057	0.058	0.058
L _x	0.013	-0.015	-0.007	-0.003
L _y	0.006	-0.008	0.004	0.01
L _z	0.05	-0.054	-0.057	-0.057
$\sqrt{\langle J^2 \rangle}$	4.38	4.40	4.39	4.40

Table 5 Spin S, orbital moment L and their composition (J) for the four magnetic atoms of the $\{\text{Co}_4\}$ core. The data are reported in units of μ_B .

	Co ₁	Co ₂	Co ₃	Co ₄
$\sqrt{\langle S^2 \rangle}$	2.56	2.56	-2.57	-2.58
S _x	-0.19	1.92	-1.92	0.975
S _y	1.355	1.6	-1.62	-0.72
S _z	-2.61	-0.56	-0.52	2.29
$\sqrt{\langle L^2 \rangle}$	0.15	0.14	0.46	0.35
L _x	-0.004	0.121	-0.33	0.057
L _y	0.051	0.065	-0.33	0.06
L _z	-0.14	-0.033	-0.033	0.33
$\sqrt{\langle J^2 \rangle}$	2.71	2.71	3.03	2.92

3.6 Exchange coupling

In order to ascertain the strength of the (anti)ferromagnetic coupling in the two complexes we computed the exchange coupling parameters (J_i) from first-principles total energies by considering the five lowest-energy spin configurations of the molecules (*uudd*, *udud*, *uddu*, *uudd*, *uuuu*) as explained in Section 2.1. The calculated exchange parameters are reported in Table 6, where positive and negative values correspond to ferromagnetic (FM) or antiferromagnetic (AFM) coupling. The parameters have been obtained either in the LDA+U approximation or including SOC in the calculation (with spin along the easy-axis direction).

The LDA+U simulations give J that are of the same order of magnitude of those extracted from experimental susceptibility (see ESI), and are in fair agreement with those reported in Ref.²⁰ for a three- J model. Both J_1 and J_2 are negative, confirming the antiferromagnetic coupling between not equivalent atoms. One of the other two parameters describing the coupling between equivalent atoms (J_3 and J_4) is positive (FM), in agreement with the data extracted from the experiments. The overall exchange interaction, estimated as the average of the J_s (-3.7 meV for $\{\text{Co}_4\}$ and -1.4 for $\{\text{Mn}_4\}$), is AFM for both molecular complexes.

The strongest J_n (J_1 in $\{\text{Co}_4\}$, J_2 in $\{\text{Mn}_4\}$) corresponds to the interaction between the two pairs of not-equivalent ions and it is related to the energy difference between the AFM ground state and the high spin FM state ($S=12$ for $\{\text{Co}_4\}$ and $S=20$ for $\{\text{Mn}_4\}$) which is larger for $\{\text{Co}_4\}$. The FM interaction between equivalent ions (intra-pair) is, instead, smaller for $\{\text{Co}_4\}$. The latter governs

the transition to low-spin FM states (for example *uudd*) which influences the behavior of the magnetization at low fields and low temperatures, hence explaining the observed switching with temperature of the magnetization curves $M(B)$ of the two molecules (Fig. 3). To further explore this behavior, we have exploited a model Heisenberg Hamiltonian with J parameters and g -factor fitted from the experimental low-field susceptibility (ESI) and used them to calculate $M(B)$ at two different temperatures. We find that the observed (Fig. 3) switch of $M(B)$ with temperature is an effect of the more marked AFM character of $\{\text{Mn}_4\}$ giving rise to a positive curvature of $M(B)$ at low field/low T. At high field/high T, instead, the most relevant factor is the larger saturation value of the magnetization in $\{\text{Mn}_4\}$ compared to $\{\text{Co}_4\}$. By increasing the range of the magnetic field beyond the experimental one, a crossing of the two theoretical curves is observed due to the combination of these two aspects (ESI).

The inclusion of SOC in the calculation leads to J_s with a sign that reflects the *uudd* magnetic order of the ground state, i.e. AFM (FM) coupling between M1/M4 and M2/M3 non-equivalent (M1/M2 and M3/M4 equivalent) ions. Nevertheless, the exchange parameters obtained with SOC are too large compared to those extracted from the experiments, suggesting that the electronic correlation can not be neglected for a reliable estimate of the strength of the magnetic interactions.

For a deeper insight of the exchange interaction, we have computed the exchange parameters also with the Liechtenstein-Katsnelson-Antropov-Gubanov (LKAG) formula³³ implemented in the TB2J package³⁴, which treats the local spin rotation of the numerical atomic orbitals for the magnetic atoms as a perturbation. The J_s evaluated with this approach present the same overall trend as those computed from total energies (Table 6), for both LDA+U and SOC case, and are reported in the ESI.

The different predictions of the various approximations (LDAU or SOC) are a consequence of the complexity of the magnetic potential energy landscape of these molecular complexes. A small perturbation (geometry, electron correlation, spin alignment) can drive the results out of equilibrium and towards a different local minimum. Despite these difficulties, all the computed J parameters predict the experimentally observed *uudd* ground state, regardless of the approach (total energies or perturbative) and inclusion of correlations or SOC. This has been verified by feeding the computed J in the Heisenberg Hamiltonian and computing the various spin configurations (ESI).

Finally, we used all the computed J parameters as input for spin dynamics simulations³⁵⁻³⁷ to predict the magnetic susceptibility, finding a good agreement with experiment in the LDA+U case (ESI). The results obtained without U correction are, instead, in striking contradiction with experiments, confirming the importance of taking into account electron correlation in the transitional metal sites.

4 Conclusions

Through a joint experimental and theoretical analysis we have characterized the properties of two coordination complexes, $\{\text{Mn}_4\}$ and $\{\text{Co}_4\}$, that display the same chemical structure but different inner magnetic core formed by Mn and Co atoms, respec-

Table 6 Exchange coupling parameters (J_i , meV) of $\{\text{Mn}_4\}$ and $\{\text{Co}_4\}$ molecular complexes extracted from DFT calculations with either LDA+U or SOC included. S is normalized to 1.

LDA + U (meV)	J_1	J_2	J_3	J_4
$\{\text{Mn}_4\}$	-0.2	-0.9	-0.2	0.9
$\{\text{Co}_4\}$	-1.8	-0.19	0.8	-0.6
SOC (meV)	J_1	J_2	J_3	J_4
$\{\text{Mn}_4\}$	-5.0	-4.2	9.3	31.8
$\{\text{Co}_4\}$	-7.35	-1.42	2.58	5.52

tively. The theoretical analysis was performed under different approximations (LDAU, SOC) and methods (first-principles, model Hamiltonians, perturbation theory).

The experimental data and the theoretical calculations show that by changing the magnetic core it is possible to tune the strength of the magnetic interaction inside the molecules and thus the robustness of the AFM configuration in an external magnetic field. Moreover, the different magnetic properties of the two chemical species lead to a different spatial extension of the magnetic moment and electronic charge density on the ligands, which influences the interaction with foreign systems and affects the efficiency of the two compounds when employed for magnetic functionalization.

We find and explain an unusual switch with temperature of the dependence of the magnetic moment from the applied magnetic field $M(B)$ for the two molecules. We relate it to two competing effects: the stronger AFM coupling in $\{\text{Mn}_4\}$ and the large value of magnetization in $\{\text{Mn}_4\}$ which dominate at low and high temperature, respectively.

The calculations clarify the role of spin-orbit effects: negligible in $\{\text{Mn}_4\}$ and relevant in $\{\text{Co}_4\}$, showing that SOC has to be considered for a reliable theoretical description of the magnetic moments of the latter. In perspective of future exploitation of these compounds in spintronics the SOC effects found in $\{\text{Co}_4\}$ should be taken into account as possible source of spin decoherence.

Our study of the exchange coupling parameters and spin dynamics demonstrate that it is necessary to explicitly include electron correlations (for instance, via a Hubbard U parameter) to properly recover these properties. The complete description of the molecular complexes can only be performed in a framework in which electronic correlation and SOC are treated on the same footing.

Conflicts of interest

There are no conflicts to declare.

Acknowledgements

The authors thank Natalya Izarova for acquisition of the crystallographic data, Brigitte Jansen for acquisition of the TGA data and Christina Houben for acquisition of some of the SQUID data. The Authors acknowledge financial support of the NFFA infrastructure under Project ID-753. Computational resources were provided by the Red Espanola de Supercomputation through a the projects FI-2019-2-0038 and FI-2020-1-0022 on Marenostrum

High Performance cluster. We acknowledge PRACE for awarding us access to MareNostrum4 at Barcelona Supercomputing Center (BSC), Spain (OptoSpin project id. 2020225411). ZZ acknowledges financial support by the Ramon y Cajal program RYC-2016-19344 (MINECO/AEI/FSE, UE) and the Netherlands Sector Plan program 2019-2023. PO, HX and ZZ thank the support by the EU H2020-NMBP-TO-IND-2018 project "INTERSECT" (Grant No. 814487), the EC H2020-INFRAEDI-2018-2020 MaX "Materials Design at the Exascale" CoE (grant No. 824143), Spanish AEI Grant Fis2015-64886-C5-38, Severo Ochoa (SEV-2017-0706) and Generalitat de Catalunya (CERCA program and Grant 201756R1506).

Notes and references

- 1 M. Ganzhorn and W. Wernsdorfer, *Molecular Magnets*, Springer, Berlin, Heidelberg, 2014.
- 2 E. Coronado, *Nat. Rev. Mater.*, 2020, **5**, 87–104.
- 3 M. Gobbi, M. A. Novak and E. Del Barco, *Journal of Applied Physics*, 2019, **125**, 240401.
- 4 D. Maniaki, E. Pilichos and S. P. Perlepes, *Front. Chem.*, 2018, **6**, 461.
- 5 L. Bogani and W. Wernsdorfer, *Nature Mater.*, 2008, **7**, 179–186.
- 6 Z. Zanolli, R. Leghrib, A. Felten, J.-J. Pireaux, E. Llobet and J.-C. Charlier, *ACS Nano*, 2011, **5**, 4592–4599.
- 7 Z. Zanolli and J.-C. Charlier, *ACS Nano*, 2012, **6**, 10786–10791.
- 8 H. Oshio and M. Nakano, *Chem. - Eur. J.*, 2005, **11**, 5178–5185.
- 9 S. Brooker and J. A. Kitchen, *Dalton Trans.*, 2009, 7331–7340.
- 10 K. S. Pedersen, J. Bendix and R. Clerac, *Chem. Commun.*, 2014, **50**, 4396–4415.
- 11 T. Jungwirth, X. Marti and P. Wadley, *Nature Nanotech*, 2016, **11**, 231–241.
- 12 M. Bragato, S. Achilli, F. Cargnoni, D. Ceresoli, R. Martinazzo, R. Soave and M. I. Trioni, *Materials*, 2018, **11**, 2030.
- 13 N. Makoto, H. Satoru, K. Hiroaki, Y. Yuki, M. Yukitoshi and S. Hitoshi, *Nature Communications*, 2019, **10**, 4305.
- 14 X.-X. Fu, F. Wei, Y. Niu and C.-K. Wang, *Physica E: Low-dimensional Systems and Nanostructures*, 2021, **131**, 114737.
- 15 V. Baltz, A. Manchon, M. Tsoi, T. Moriyama, T. Ono and Y. Tserkovnyak, *Rev. Mod. Phys.*, 2018, **90**, 015005.
- 16 R. Frielinghaus, C. Besson, L. Houben, A.-K. Saelhoff, C. M. Schneidera and C. Meyer, *RCS Adv.*, 2015, **5**, 84119.
- 17 C. Besson, P. Stegmann, M. Schnee, Z. Zanolli, S. Achilli, N. Wittemeier, A. Vierck, R. Frielinghaus, P. Kögerler, J. Maultzsch, P. Ordejón, C. M. Schneider, A. Hucht, J. König and C. Meyer, *arXiv:2107.07723*, 2021.
- 18 A. Ardavan, O. Rival, J. J. L. Morton, S. J. Blundell, A. M. Tyryshkin, G. A. Timco and R. E. P. Winpenny, *Phys. Rev. Lett.*, 2007, **98**, 057201.
- 19 M. Murrie, *Chem. Soc. Rev.*, 2010, **39**, 1986–1995.
- 20 E. Kampert, F. F. B. J. Janssen, D. W. Boukhvalov, J. C. Russ-

- cher, J. M. M. Smits, R. de Gelder, B. de Bruin, P. C. M. Christianen, U. Zeitler, M. I. Katsnelson, J. C. Maan and A. E. Rowan, *Inorg. Chem.*, 2009, **48**, 11903–11908.
- 21 J. M. Soler, E. Artacho, J. D. Gale, A. García, J. Junquera, P. Ordejón and D. Sánchez-Portal, *J. Phys.: Condens. Matter*, 2002, **14**, 2745.
- 22 A. García, N. Papior, A. Akhtar, E. Artacho, V. Blum, E. Bosoni, P. Brandimarte, M. Brandbyge, J. I. Cerdá, F. Corsetti, R. Cuadrado, V. Dikan, J. Ferrer, J. Gale, P. García-Fernández, V. García-Suárez, S. García, G. Huhs, S. Illera, R. Korytár, P. Koval, I. Lebedeva, L. Lin, P. López-Tarifa, S. G. Mayo, S. Mohr, P. Ordejón, A. Postnikov, Y. Pouillon, M. Pruneda, R. Robles, D. Sánchez-Portal, J. M. Soler, R. Ullah, V. Wen-zhe Yu and J. Junquera, *J. Chem. Phys.*, 2020, **152**, 204108.
- 23 W. Kohn and L. J. Sham, *Phys. Rev. B*, 1965, **140**, A1133.
- 24 D. M. Ceperley and B. J. Alder, *Phys. Rev. Lett.*, 1980, **45**, 566.
- 25 A. M. Ritzmann, M. Pavone, A. B. Muñoz García, J. A. Keith and E. A. Carter, *J. Mater. Chem. A*, 2014, **2**, 8060–8074.
- 26 R. Cuadrado, R. Robles, A. García, M. Pruneda, P. Ordejón, J. Ferrer and J. I. Cerdá, *to be published*.
- 27 Z. Zanolli, C. Niu, G. Bihlmayer, Y. Mokrousov, P. Mavropoulos, M. J. Verstraete and S. Blügel, *Phys. Rev. B*, 2018, **98**, 155404.
- 28 N. F. Chilton, R. P. Anderson, L. D. Turner, A. Soncini and K. S. Murray, *Phys. Rev. Lett.*, 2013, **34**, 1164.
- 29 G. A. Bain and J. F. B. Berry, *J. Chem. Ed.*, 2008, **85**, 532–536.
- 30 F. Lloret, M. Julve, J. Cano, R. Ruiz-García and E. Pardo, *Inorganica Chimica Acta*, 2008, **361**, 3432–3445.
- 31 J.-P. Launay and M. Verdaguer, *Electrons in molecules*, Oxford University Press, 2014.
- 32 R. Cuadrado and J. I. Cerdá, *J. Phys. Condens. Mat.*, 2012, **24**, 086005.
- 33 A. I. Liechtenstein, M. I. Katsnelson, V. P. Antropov and V. A. Gubanov, *Journal of Magnetism and Magnetic Materials*, 1987, **67**, 65–74.
- 34 X. He, N. Helbig, M. J. Verstraete and E. Bousquet, *Computer Physics Communications*, 2021, **264**, 107938.
- 35 L. Landau and E. Lifshitz, *Perspectives in Theoretical Physics*, Elsevier, 1992, pp. 51–65.
- 36 T. L. Gilbert, *IEEE transactions on magnetics*, 2004, **40**, 3443–3449.
- 37 X. Gonze, B. Amadon, G. Antonius, F. Arnardi, L. Baguet, J.-M. Beuken, J. Bieder, F. Bottin, J. Bouchet, E. Bousquet *et al.*, *Computer Physics Communications*, 2020, **248**, 107042.

Supplementary information: Magnetic properties of $\{M_4\}$ coordination clusters with different magnetic cores (M=Co, Mn).

Simona Achilli,^{*ab} Claire Besson,^c Xu He,^d
Pablo Ordejón,^d Carola Meyer^e, Zeila Zanolli^{f,b,d}

^a Dipartimento di Fisica "Aldo Pontremoli", Università degli Studi di Milano, Via Celoria 16, Milan, Italy, simona.achilli@unimi.it

^b European Theoretical Spectroscopy Facilities.

^c Department of Chemistry, The George Washington University, Washington DC 20052, USA.

^d Catalan Institute of Nanoscience and Nanotechnology (ICN2), CSIC and BIST, Campus UAB.

^e Department of Physics, Universität Osnabrück, 49076 Osnabrück, Germany.

^f Chemistry Department, Debye Institute for Nanomaterials Science, Condensed Matter and Interfaces, Utrecht University, PO Box 80 000, 3508 TA Utrecht, The Netherlands.

1 Synthesis and characterization

1.1 Materials and synthesis

2-aminophenol (> 98%, TCI) was recrystallised from boiling water, washed with ice-cold water and diethylether and stored under inert atmosphere. 2,6-diacetylpyridine (> 98%, TCI), Co(OAc)₂·4 H₂O (99.999% trace metal basis, Aldrich) and Zn(OAc)₂·2 H₂O (99.999% trace metal basis, Aldrich) were used as received. Solvents were, when indicated, deaerated by three freeze-pump-thaw cycles using argon as inert gas. PE spatulas and PTFE cannulas were employed to avoid magnetic contamination of the samples.

[Mn₄OAc₄L₂] (H₂L=2,6-bis-(1-(2-hydroxyphenyl)iminoethyl)pyridine) ({Mn₄})

The complex was synthesized according to the literature.[?]

[Co₄L₂(OAc)₄] (H₂L = 2,6-bis-(1-(2-hydroxyphenyl)iminoethyl) pyridine) ({Co₄})

Synthesis of the complex follows the preparation of the manganese analogue,[?] with some modifications. In particular, conducting the reaction under protective atmosphere is necessary to avoid the formation of an unidentified brown precipitate by the reaction of 2-aminophenol, cobalt acetate and dioxygen. 2,6-diacetylpyridine (439 mg, 2.5 mmol, 1 eq.), 2-aminophenol (583 mg, 5.3 mmol, 2.2 eq.) and Co(OAc)₂·4 H₂O (1.33 g, 5.3 mmol, 2.2 eq.) were introduced in a Schlenk flask under argon. Deaerated methanol (10 mL) was canulated into the flask and the resulting red solution was refluxed under argon for two hours. After the solution was returned to room temperature, deaerated diethylether (100 mL) was canulated in and allowed to mix with the solution, yielding an orange microcrystalline precipitate. The solid was filtered and washed with diethylether (3×30 mL) to yield Co₄L₂(OAc)₄·4 CH₃CN (1.0-1.2 g, 0.8-0.9 mmol, 60-70 %) as a dark orange powder. The compound was recrystallised by dissolving the solid (130 mg, 0.1 mmol) in acetonitrile (25 mL), sonicating and filtering solution and setting it up for gas phase diffusion of diethylether. Dark red crystals of Co₄L₂(OAc)₄·4 CH₃CN (65-100 mg, 50-75 % recrystallisation yield) were collected by filtration after 3-4 days and used for all further characterization and reactions.

UV (CH₃CN) λ_{max} , nm (log ϵ): 260sh (4.50), 321 (4.27), 398 (4.14).

CV $E_{1/2}$, V vs. Fc⁺/Fc: 0.30, 0.80.

TGA (N₂, 10 K.min⁻¹) -12.3 % (50-150 K, -4 CH₃CN (th. -12.4 %)). -30.5 % (350-400 K), -9.4 % (400-520 K).

Single crystal diffraction quality material can be obtained by gas phase diffusion of *n*-pentane into a saturated ethanol solution. The compound crystallizes in the P4/n space group with ethanol as a solvate. Due to twinning of the crystals and disorder of the solvate molecules we were only able to refined to a wR^2 of 36 %. The asymmetric unit unequivocally contains a Co₄L₂(OAc)₄ molecule and an ethanol molecule hydrogen bound to one of the acetate oxygens, as well as a second ethanol molecule which refines satisfactorily with a two-parts disorder of the hydroxyl group with approximately equal occupancies. The SQUEEZE routine was used to account for the residual electronic density localised in the large voids of the unit cell, which corresponds to 8 ethanol molecules per unit cell, yielding a final wR^2 of 36 % ($R_1 = 18$ %) with a formula Co₄L₂(OAc)₄·3 EtOH. Crystal structure data is available from Cambridge Structural Database, under CCDC number 1855019.

$\text{Zn}_4\text{L}_2(\text{OAc})_4$ ($\text{H}_2\text{L} = 2,6\text{-bis-(1-(2-hydroxyphenyl)iminoethyl) pyridine}$) ($\{\text{Zn}_4\}$)

Synthesis of the complex follows the preparation of the manganese analogue,⁷ with some modifications. Specifically, 2,6-diacetylpyridine (186 mg, 1.0 mmol, 1 eq.), 2-aminophenol (250 mg, 2.3 mmol, 2.3 eq.) and $\text{Zn}(\text{OAc})_2 \cdot 2 \text{H}_2\text{O}$ (501 g, 2.3 mmol, 2.3 eq.) were introduced in a Schlenk flask under argon. Deaerated methanol (10 mL) was catalyzed into the flask and the resulting yellow solution was refluxed under argon for two hours. Note that this step can be conducted in air, but in that case a small amount of strongly red-colored 2-amino-3H-phenoxazin-3-one is formed by the oxidative dimerisation of 2-aminophenol and contaminates the product obtained before recrystallisation. After the solution was returned to room temperature, a microcrystalline yellow solid was precipitated by the addition of diethylether (200 mL). The solid (590-640 mg) was filtered, washed with diethylether (4×25 mL), and redissolved in chloroform (100 mL). Pentane was allowed to diffuse in the solution from the gas phase (to accelerate the process, the solution was divided in three fractions). Yellow single crystal diffraction quality $\text{Zn}_4\text{L}_2(\text{OAc})_4 \cdot 4.5\text{CHCl}_3$ (350-400 mg, 40-45 % yield) was collected by filtration after 3-4 days and used for all further characterization and reactions.

The compound crystallised in the $\text{P2}_1/\text{n}$ space group, with 4.5 CHCl_3 molecules and a $\text{Zn}_4\text{L}_2(\text{OAc})_4$ complex in the asymmetric unit. One of the chloroform molecules is located close to the inversion center at (0, 0.5, 0) and has an occupancy of 0.5. Another could be refined as an approximately 1:1 disorder between two close positions. Residual electronic density lies mostly in close proximity with the chlorine atoms of the other chloroform molecules, but attempts at refining similar disorder yielded only small occupancy factors and no significant improvement of the R factors, and were abandoned, leaving a final wR^2 factor of 12 % ($R_1 = 4.3\%$). Crystal structure data is available from Cambridge Structural Database, under CCDC number 1855020.

UV (CH_3CN) λ_{max} , nm ($\log \epsilon$): 265sh (4.40), 293 (4.23), 346 (4.17), 407 (4.23).

SQUID: χ_{dia} , $\text{m}^3 \cdot \text{mol}^{-1}$ ($\text{emu} \cdot \text{mol}^{-1}$): -5.3×10^{-9} (4.2×10^{-4}).

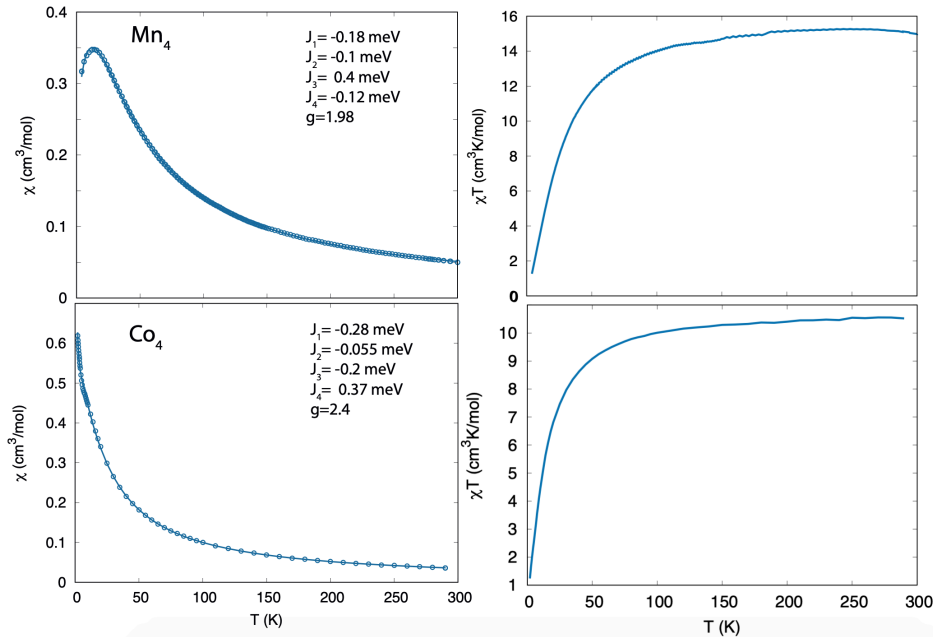


Figure 1: Left panels: Experimental (dots) magnetic susceptibility (χ cm³/mol) of {Mn₄} and {Co₄} with the relative fit (line). The J derived from fitting are reported as inset together with the value of g . Right panels: experimental susceptibility times temperature ($\chi \times T$, cm³K/mol) of {Mn₄} and {Co₄} as a function of the temperature.

2 Fit of SQUID data

The experimental magnetic susceptibility was fitted exploiting an Heisenberg model Hamiltonian in which the exchange coupling parameters between pairs of ions are left as free parameters. The fit functions are reported in Figure 1 as solid lines, together with the experimental data (points) and the J_n extracted from the fit.

The J_n obtained are in fair agreement with those extracted from the LDA+U calculation. The fitted g -factor is ~ 2 in {Mn₄} confirming the validity of the spin-only approximation, while it deviates from 2 in {Co₄} reflecting the role of SOC.

Through the model Hamiltonian with parameters obtained from the fit of the experimental data the magnetization was calculated at different temperatures and fields. For large fields or large temperatures the magnetization of {Mn₄} is larger than that of {Co₄}, as observed in the experiments. The saturation value ($gS\mu_B$) of {Mn₄} ($20\mu_B$) is indeed larger than for {Co₄} ($12\mu_B$ in a spin-only model). At low temperature, fields of 20 T for {Co₄} and 25 T for of {Mn₄} are needed for the magnetization to reach saturation. These values are significantly large compared to the fields accessible in our experiments (Fig. 3 in the main text).

In the low field–low-temperature limit the model shows an inversion of the magnetization curves leading to larger magnetization of {Co₄} with respect to {Mn₄}. Moreover the two curves display opposite curvature, in agreement with SQUID data at low temperature. In particular, the magnetization of {Mn₄} shows positive curvature, as expected for an antiferromagnet, while for {Co₄} an almost linear dependence on the field can be observed.

The slope of the magnetization is an indication of the coupling between the magnetic centers: the stronger the antiferromagnetic coupling, the smaller the slope. Moreover, the smaller the moment per atom, the stronger the linear dependence of M on the field. Both these aspects explain the fast rise observed for the magnetization of {Co₄} in the experimental data, as due to the smaller value of S (or J) (see table 4 and 5 in the main text) and of the AFM coupling, with respect to {Mn₄}. On the other hand, the saturation value for the magnetization of {Co₄} is smaller than for {Mn₄}, thus the two magnetization curves show a crossing for a certain value of the field which is not reached in the experiments. At high temperature the magnetization curves flatten, resulting in a slower growth as a function of the field with respect to the low temperature limit. The linear dependence on the field $M = Ng^2S(S+1)\mu_B^2B$ in this case is governed by the value of S and it is smaller for {Co₄} than for {Mn₄}, in agreement with what observed in the experiments at high temperature.

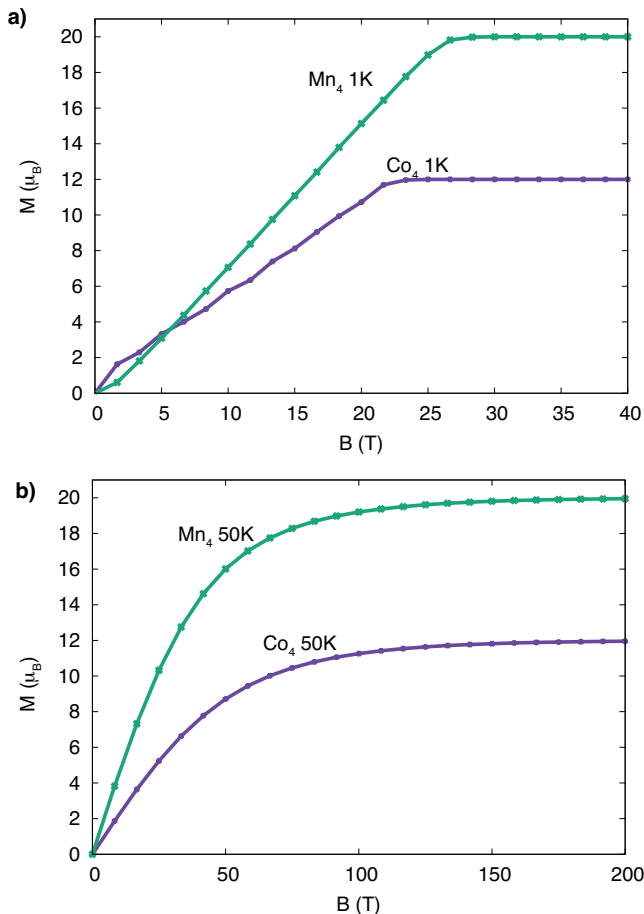


Figure 2: Magnetization versus field dependence for $\{\text{Mn}_4\}$ and $\{\text{Co}_4\}$ at 1 K (a) and 50 K (b).

3 Exchange parameters from different calculations

The exchange parameters were extracted by fitting a system of equations for the five lowest energy spin configurations of the molecule, as reported in the main text. For a comparison with the available experimental data and previous theoretical calculations on $\{\text{Mn}_4\}$ we consider also a set of only three J parameters, despite we retain this choice less accurate. Indeed the assumption $J_3 = J_{(1,2)} = J_{(3,4)}$ is not correct, as the M_1/M_2 and M_3/M_4 pairs are not equivalent in terms of chemical coordination and ligands groups. The obtained values are reported in Tables 1. For a system of three exchange parameters, we recover the experimental results of Kampert *et al.* [?].

In addition, we also computed the J values with the Liechtenstein-Katsnelson-Antropov-Gubanov (LKAG) formula [?] implemented in the TB2J package. [?]

Table 1: Computed exchange parameters J (meV and Kelvin) for the $\{\text{Mn}_4\}$ molecular complex, using LDA+U and a three- J Heisenberg model. The experimental values from Ref. [?] are reported for comparison

J	J_1 (1-4,2-3)	J_2 (1-3,2-4)	J_3 (1-2, 3-4)
$\{\text{Mn}_4\}$ (meV)	-0.7	-0.4	-0.2
$\{\text{Mn}_4\}$ (Kelvin)	-8.1	-4.1	-2.0
Exp [?] (Kelvin)	-2.2	-1.1	-0.1

TB2J evaluates the J for each couple of atoms. So there are six J parameters. The non-equivalent J for pairs M_1/M_3 and M_2/M_4 is related to the not perfect symmetry of the electronic structure associated with these pairs of atoms, probably due to some orbital polarization in the Mn/Co.

When the Heisenberg equation is solved for four exchange parameters, the TB2J results for the LDA+U case give the same trend obtained using SIESTA total energies: the ferromagnetic coupling between atoms M_1 and M_2 is not reproduced ($J_3 < 0$) and the exchange coupling parameters are larger for $\{\text{Co}_4\}$ than for $\{\text{Mn}_4\}$. With SOC included, the exchange parameters obtained with TB2J are in fair agreement with those reported in the main text supporting the robustness of the

Table 2: J of the $\{\text{Mn}_4\}$ and $\{\text{Co}_4\}$ molecular complexes obtained with TB2J in LDA+U and with SOC included. The values are reported in meV.

LDA+U	J_1 (1-4,2-3)	J_2 (1-3,2-4)	J_3 (1-2)	J_4 (3-4)
$\{\text{Mn}_4\}$	-1.21/-1.23	-1.77/-1.84	-0.8	0.1
$\{\text{Co}_4\}$	-3.47/-3.29	-1.70/-1.82	0.03	-2.25
SOC	J_1 (1-4,2-3)	J_2 (1-3,2-4)	J_3 (1-2)	J_4 (3-4)
$\{\text{Mn}_4\}$	-34.5/1.3	-55.7/-29.2	12.94	3.29
$\{\text{Co}_4\}$	-3.24/-5.09	-11.84/-10.68	1.18	18.35

results. The comparison between the two molecules confirms indeed the larger strength of the magnetic coupling in $\{\text{Mn}_4\}$ with respect to $\{\text{Co}_4\}$ but the absolute value of the J is too large.

All the methods agree in the qualitative description of the magnetic coupling within the two molecules and in these terms, i.e. only qualitatively, these parameters should be taken into account.

4 Spin dynamics calculation

Using the Heisenberg model constructed from DFT results, we perform Ginzberg-Landau-Lifshitz (GLL) atomic spin dynamics^{??} (ASD) to compute the magnetic susceptibility with the MULTIBINIT code[?]. The isothermal magnetic susceptibility is calculated with the fluctuation-dissipation theorem[?]:

$$\chi = \frac{1}{k_B T} (\langle m^2 \rangle - \langle m \rangle^2), \quad (1)$$

where $\langle \rangle$ means the average over the ensembles, m is the magnetization of the system.

Four sets of parameters from DFT results with either SOC or Hubbard U correction, computed by total energy (TE) method or TB2J, were used as input. Another set of exchange parameters by fitting to experimental data is also taken as comparison. The results are shown in Fig. 3.

The "λ"-shape of the susceptibility curves are similar to extended structures, where the susceptibility diverges at the critical temperature, which is ill-defined in molecules. Nevertheless the temperature of the peak (defined as T_P), the decay of the susceptibility above the T_P , and the value of the susceptibilities, all shows that the exchange parameters from the DFT results with the "+U" correction agrees better with experiments, in which the exchange values are smaller in general.

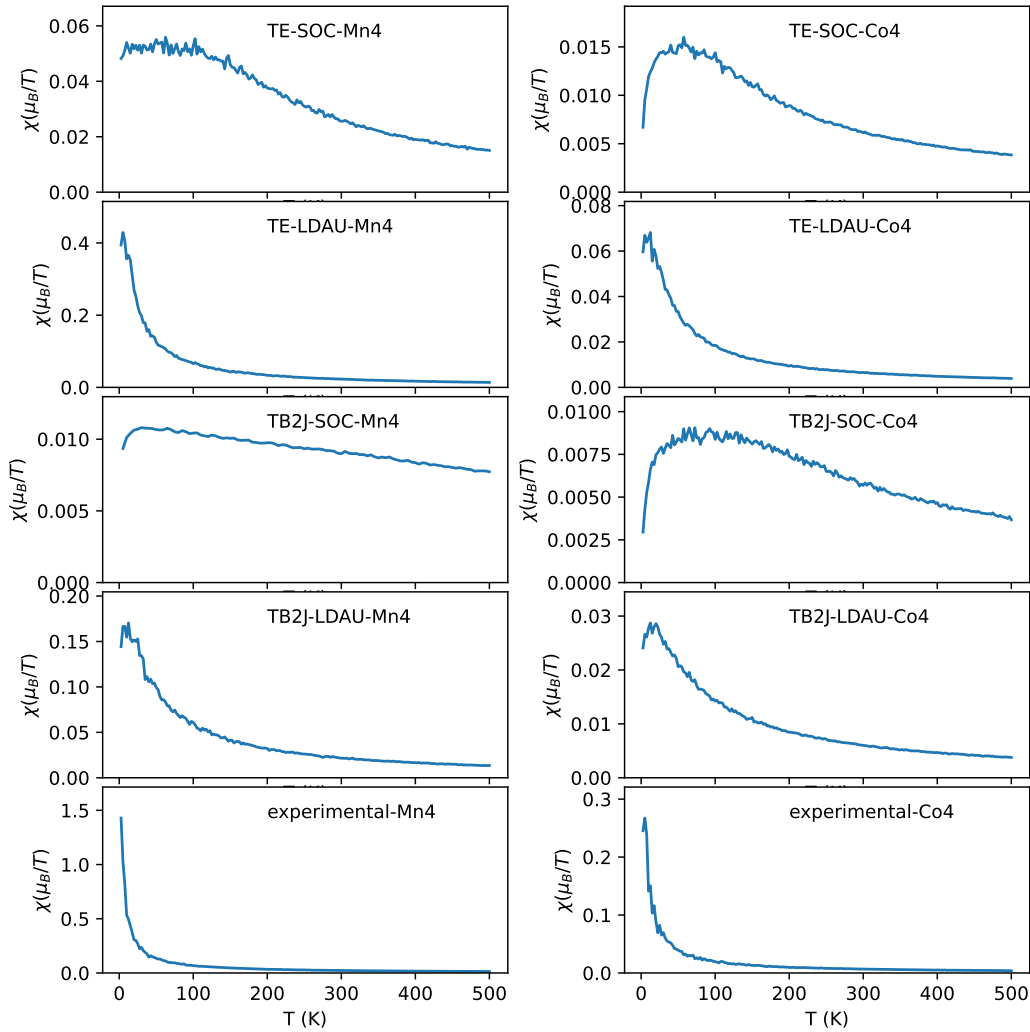


Figure 3: The susceptibilities computed with spin dynamics using various set of parameters. TE-SOC: fit from DFT (with SOC) energies. TE-LDAU: fit from DFT (with +U correction). TB2J-SOC: computed with TB2J from DFT with SOC. TB2J-LDAU: computed from TB2J with DFT+U. Experimental: fit from experimental data. The left and the right panels are from Mn4 and Co4, respectively.

5 Relaxed structures

The atomic coordinates (in Å) obtained through structural relaxation performed in DFT-LDA and SOC included are reported below for {Co₄} and {Mn₄}.

{Co₄}:

Co 11.784660 24.970504 9.657395
Co 10.497270 22.083542 10.349018
Co 13.826910 22.493219 9.595356
Co 11.640250 22.424358 7.355454
O 12.276659 23.190641 10.768667
O 13.053111 23.738692 8.233238
O 12.150853 21.350956 8.965670
O 10.536075 23.509294 8.730816
N 11.150917 25.250576 11.697139
N 10.234291 26.256309 9.631992
N 11.898964 25.955696 7.819901
C 12.573409 23.459183 12.047217
C 13.501743 22.727320 12.800231
H 14.089320 21.934242 12.292846
C 13.683728 23.040467 14.147378
H 14.424537 22.471937 14.743995
C 12.967844 24.084895 14.745447
H 13.125847 24.329670 15.812985
C 12.094520 24.862400 13.986050
H 11.619728 25.748710 14.442161
C 11.894341 24.565336 12.624100
C 10.126773 26.025442 11.948916
C 9.578037 26.345785 13.287772
H 10.175627 27.151091 13.781884
H 8.530036 26.715922 13.221056
H 9.604646 25.444738 13.951800
C 9.538585 26.565027 10.740648
C 8.341386 27.295098 10.668957
H 7.820799 27.608225 11.593808
C 7.833021 27.630308 9.415343
H 6.862677 28.154484 9.327204
C 8.583412 27.341326 8.274367
H 8.239272 27.639455 7.265994
C 9.816490 26.700082 8.429924
C 10.790725 26.483101 7.373647
C 10.499096 26.837914 5.965518
H 11.118355 26.205940 5.283527
H 9.420716 26.654751 5.742013
H 10.706556 27.914849 5.751836
C 13.024326 25.741449 7.058258
C 13.537168 26.594422 6.071137
H 13.031246 27.555676 5.858676
C 14.722039 26.250453 5.422129
H 15.143996 26.930256 4.657679
C 15.384636 25.058139 5.746152
H 16.319763 24.794952 5.214912
C 14.880653 24.193928 6.719788
H 15.372314 23.234492 6.981271
C 13.696788 24.537235 7.377188
N 11.408346 20.414618 11.203267
N 10.045893 22.163800 12.313801
N 8.804952 23.397905 10.567973
C 12.292475 20.027330 9.077568
C 12.842500 19.207261 8.088787
H 13.105214 19.659644 7.110727
C 13.063406 17.859247 8.376878
H 13.502886 17.200660 7.602911

C 12.747203 17.325275 9.633942
H 12.915108 16.251224 9.840454
C 12.205322 18.140545 10.625957
H 11.907104 17.720989 11.605658
C 11.969344 19.493931 10.348564
C 11.650265 20.474168 12.485497
C 12.636444 19.653283 13.225367
H 13.450079 19.328860 12.531885
H 13.088399 20.253265 14.051051
H 12.169384 18.748781 13.685771
C 10.832454 21.468847 13.158681
C 10.796516 21.686320 14.539889
H 11.495754 21.142632 15.202811
C 9.837013 22.560233 15.053198
H 9.769746 22.736793 16.143428
C 8.934736 23.169554 14.182981
H 8.097913 23.779891 14.572506
C 9.094103 22.979726 12.800664
C 8.331740 23.643350 11.763572
C 7.163003 24.495043 12.088568
H 6.207428 23.931855 11.948397
H 7.186354 24.831516 13.149891
H 7.130370 25.394655 11.423137
C 8.324216 23.904560 9.387352
C 7.023869 24.354608 9.088815
H 6.233333 24.332011 9.859428
C 6.706528 24.748870 7.789651
H 5.679835 25.092977 7.561875
C 7.661627 24.652798 6.770087
H 7.379020 24.906744 5.729114
C 8.956450 24.210011 7.041607
H 9.719280 24.084856 6.245056
C 9.303374 23.877674 8.358257
O 13.550916 25.687501 10.333671
O 14.950837 23.896252 10.435570
C 14.509448 25.023697 10.844952
C 15.140291 25.589838 12.078773
H 16.108362 25.094580 12.300594
H 15.260569 26.691401 11.992143
H 14.438239 25.391374 12.931510
O 9.264080 21.016327 9.158996
O 9.981759 21.377015 7.029957
C 9.077203 21.170511 7.908653
C 7.656352 21.159999 7.435931
H 7.600703 21.151344 6.327734
H 7.105154 20.298050 7.871949
H 7.167930 22.096305 7.813696
O 14.512862 20.887840 10.767680
O 15.138232 21.186628 8.688865
C 15.122061 20.452460 9.730707
C 15.736798 19.099933 9.768206
H 16.570752 19.090335 10.507721
H 14.961592 18.371446 10.113626
H 16.110875 18.800866 8.767205
O 12.909671 21.999680 5.790142
O 11.488189 23.663316 5.667504
C 12.484160 23.030674 5.173137
C 13.128020 23.549145 3.938469
H 14.056502 22.988709 3.703249
H 12.409620 23.476724 3.089349
H 13.369196 24.629938 4.096111

{Mn₄}

Mn 11.810113 24.985996 9.743006
Mn 10.424819 22.105112 10.320622
Mn 13.969259 22.519930 9.574551
Mn 11.607671 22.312376 7.271543
O 12.349963 23.147982 10.831958
O 13.140464 23.571435 8.098263
O 12.345050 21.326161 8.840598
O 10.496148 23.528278 8.643963
N 11.103152 25.197501 11.777895
N 10.216281 26.274131 9.676366
N 11.890695 25.881198 7.790930
C 12.598813 23.438037 12.113694
C 13.538059 22.730289 12.880143
H 14.135978 21.938064 12.381465
C 13.716597 23.053512 14.225799
H 14.466366 22.503544 14.828710
C 12.981132 24.093676 14.810091
H 13.138994 24.358651 15.873515
C 12.083104 24.839617 14.047557
H 11.583453 25.716735 14.497662
C 11.870084 24.527046 12.689523
C 10.080681 25.994708 12.005918
C 9.546066 26.368410 13.338673
H 10.158648 27.184771 13.798833
H 8.501386 26.750637 13.269521
H 9.564052 25.494243 14.036190
C 9.519736 26.565525 10.790827
C 8.322393 27.297096 10.700291
H 7.771295 27.596526 11.612739
C 7.835847 27.640072 9.438633
H 6.864361 28.162054 9.339557
C 8.588967 27.345740 8.297761
H 8.238350 27.636652 7.288881
C 9.816809 26.695904 8.461386
C 10.779240 26.441424 7.388195
C 10.469343 26.827821 5.989159
H 11.084954 26.222238 5.280743
H 9.388972 26.652695 5.766540
H 10.676751 27.911245 5.802432
C 13.005089 25.665510 7.012250
C 13.513339 26.561176 6.054061
H 12.985913 27.517018 5.868582
C 14.713268 26.281899 5.401472
H 15.114912 27.003092 4.663350
C 15.418169 25.105071 5.685767
H 16.370640 24.891407 5.162735
C 14.920698 24.193405 6.616684
H 15.436848 23.237961 6.848087
C 13.721749 24.467567 7.279225
N 11.478065 20.440099 11.180512
N 10.003855 22.178942 12.333361
N 8.775266 23.494498 10.565036
C 12.408593 19.997141 9.045486
C 12.918357 19.125851 8.079778
H 13.195354 19.548705 7.091340
C 13.081014 17.774955 8.386179
H 13.483453 17.082870 7.621038
C 12.750828 17.293427 9.659596
H 12.879629 16.219411 9.896550

C 12.245944 18.156490 10.630929
H 11.933575 17.765155 11.618521
C 12.055948 19.518712 10.336676
C 11.666559 20.505982 12.473250
C 12.631942 19.682775 13.243120
H 13.452680 19.331991 12.571416
H 13.078346 20.279745 14.074642
H 12.142121 18.787278 13.701064
C 10.810985 21.480729 13.153574
C 10.777720 21.687779 14.537103
H 11.483502 21.153446 15.201722
C 9.816902 22.561530 15.054735
H 9.761617 22.737795 16.146542
C 8.914799 23.190749 14.196371
H 8.101547 23.821929 14.604057
C 9.058508 23.008922 12.809644
C 8.310229 23.711196 11.775950
C 7.116812 24.523390 12.119889
H 6.177053 23.930361 11.983475
H 7.137163 24.854052 13.184148
H 7.048056 25.426713 11.463985
C 8.294030 23.971264 9.377957
C 6.985741 24.402518 9.078548
H 6.208726 24.395808 9.864623
C 6.645107 24.768102 7.776819
H 5.611433 25.100776 7.560535
C 7.584354 24.666278 6.741623
H 7.286273 24.909318 5.702311
C 8.882809 24.228377 7.004842
H 9.636329 24.102363 6.198341
C 9.255876 23.909629 8.319972
O 13.629165 25.693699 10.335326
O 15.054352 23.949492 10.419150
C 14.579768 25.047346 10.878908
C 15.148944 25.577028 12.154026
H 16.102522 25.070021 12.411438
H 15.283882 26.679496 12.085672
H 14.405273 25.377946 12.971604
O 9.240174 20.965235 9.109180
O 9.939535 21.279195 6.990173
C 9.017738 21.132906 7.868470
C 7.596402 21.202296 7.413526
H 7.528188 21.226430 6.305692
H 7.019675 20.346110 7.830899
H 7.143116 22.142987 7.825555
O 14.587882 20.910049 10.688605
O 15.351206 21.082424 8.631351
C 15.226349 20.400428 9.687313
C 15.757963 19.019043 9.815996
H 16.581455 19.010146 10.568026
H 14.940826 18.348605 10.182828
H 16.133811 18.655074 8.836485
O 12.967978 21.908972 5.586999
O 11.521639 23.566847 5.647444
C 12.523106 22.978168 5.081699
C 13.126088 23.607245 3.878303
H 14.073814 23.096458 3.606186
H 12.402614 23.547213 3.031790
H 13.323867 24.686749 4.095232